Review Article

Kunfeng Chen, Dongfeng Xue*

Nanofabrication strategies for advanced electrode materials

Abstract: The development of advanced electrode materials for high-performance energy storage devices becomes more and more important for growing demand of portable electronics and electrical vehicles. To speed up this process, rapid screening of exceptional materials among various morphologies, structures and sizes of materials is urgently needed. Benefitting from the advance of nanotechnology, tremendous efforts have been devoted to the development of various nanofabrication strategies for advanced electrode materials. This review focuses on the analysis of novel nanofabrication strategies and progress in the field of fast screening advanced electrode materials. The basic design principles for chemical reaction, crystallization, electrochemical reaction to control the composition and nanostructure of final electrodes are reviewed. Novel fast nanofabrication strategies, such as burning, electrochemical exfoliation, and their basic principles are also summarized. More importantly, colloid system served as one up-front design can skip over the materials synthesis, accelerating the screening rate of high-performance electrode. This work encourages us to create innovative design ideas for rapid screening high-active electrode materials for applications in energy-related fields and beyond.

Keywords: nanomaterials, lithium battery, supercapattery, combustion synthesis, colloid

*Corresponding author: Dongfeng Xue, State Key Laboratory of Rare Earth Resource Utilization, Changchun Institute of Applied Chemistry, Chinese Academy of Sciences, Changchun 130022, China, E-mail: dongfeng@ciac.ac.cn
Kunfeng Chen, State Key Laboratory of Rare Earth Resource Utilization, Changchun Institute of Applied Chemistry, Chinese Academy of Sciences, Changchun 130022, China

1 Introduction

Advanced energy storage devices, i.e., Li-ion battery, supercapacitor, need high electroactive metal oxide materials with stable structure during charging/discharging cycling [1-3]. However, metal oxide electrode materials often suffer from low conductivity, and slow ion diffusion rate during electrochemical redox reaction. In recent years, lots of efforts are done to design nanostructured materials to enhance their function. When downsizing to nanosize, the electroactive areas of materials are increased and ion/electron diffusion length is shortened, and therefore specific capacitance of active materials is significantly enhanced [4-6]. For example, 3D holey-graphene/niobia composite architectures have been designed to show ultrahigh-rate energy storage performance [7]. The highly interconnected graphene network in the 3D architecture shows excellent electron transport properties, while its hierarchical porous structure enables rapid ion transport. Although the nanostructured materials have shown extraordinary promise for electrochemical energy storage, most of the existing synthesis techniques require multistep and laborious procedures [8,9]. The dual pressure of energy needs and environmental requirements in society demand the rapid screening of exceptional performance materials to shorten R&D of advanced energy storage devices. As shown in Figure 1a, R&D of electrode materials mainly includes structure & component design, materials synthesis and performance evaluation. During these processes, materials synthesis often need longer time and complex equipments, which increase the finding time of new electrode materials. The development of easy and fast nanofabrication strategy can accelerate finding rate of new electrode materials in laboratory (Figure 1b). Furthermore, with creative design idea, the material synthesis process can be replaced or fused into one structure-performance process (Figure 1c), which not only accelerate the finding rate of new electrode materials, but also decrease the cost of searching new electrode materials.
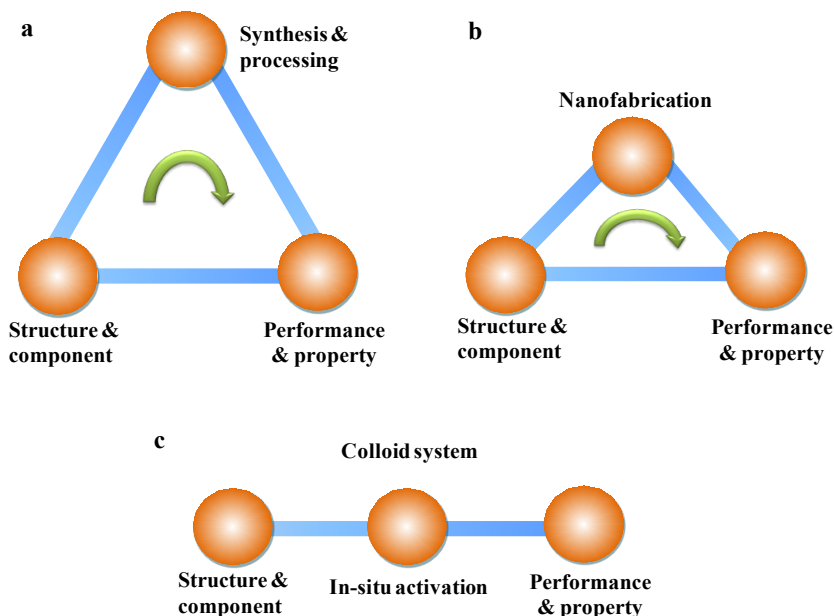
Figure 1. Research strategy of electrode materials. (a) Traditional study method, (b) fast nanofabrication increasing the screening rate of advanced electrode materials, (c) novel colloid electrode system freeing itself from the constraint of materials synthesis.

In this review, we introduced novel nanofabrication strategies for advanced electrode materials, including (1) the coupled chemical reaction and crystallization route to the polymorphic materials, (2) fast and general burning route for electrode materials synthesis, (3) fast in-situ electrochemical exfoliation for synthesizing 2D graphene materials, (4) in-situ activation of colloid electrode overcoming the materials synthesis process. These nanofabrication strategies can significantly accelerate the screening of exceptional performance materials.

2 Controllable crystal morphologies by nanofabrication

The structures and morphologies of inorganic materials can significantly affect their performances when applied in the field of electrochemical energy storage [10,11]. With the rapid progress of nanofabrication, inorganic materials with controllable morphologies, sizes and structures have been achieved [12,13]. However, how chemical reactions and crystallization process affect the morphologies and components still lacks in-depth understanding. This section focuses on the chemical reaction-controlled crystallization of Cu- and Mn-based compounds by designing vapor-, liquid- and solid-phase reactions [14,15]. Furthermore, their morphology-dependent electrochemical performances are also discussed.

2.1 Cu-based electrode materials

Cu-based materials mainly consist of three kinds of oxidation states, Cu, Cu^+ and Cu^{2+}. To synthesize different Cu-based compounds, the oxidation reaction ($Cu \rightarrow Cu_2O \rightarrow CuO$) or reduction reaction ($CuO \rightarrow Cu_2O \rightarrow Cu$) need to be controlled [16-18]. The equilibrium constant and extent of redox reaction can be calculated according to electromotive force. The standard equilibrium constant of a chemical reaction can be expressed as:

$$K^{\Theta}(T) = \exp[-\Delta_r G_m^{\Theta}(T) / RT] ,$$

$$\Delta_r G_m^{\Theta}(T) = -RT \ln K^{\Theta}(T) \quad (1)$$

where K^{Θ} is equilibrium constant, $\Delta_r G_m^{\Theta}$ is Gibbs free energy, T is temperature, R is molar gas constant. When $\Delta_r G_m = 0$, $E = 0$,

$$\ln K^{\Theta} = \frac{zFE_{MF}^{\Theta}}{RT} \quad (2)$$

It is shown that the equilibrium constant of the redox reaction is only related to the standard electromotive force. The larger the electromotive force is, the greater the equilibrium constant of the redox reaction, and the more complete the forward reaction is. Besides the redox reaction, coordination, hydrolysis, precipitation, and acid-base neutralization reactions can also influence the synthesis of Cu-based compounds [19-21].

As shown in Figure 2a, Cu-based compounds with different compositions and morphologies can be obtained by controlling the chemical reaction and crystallization process [22]. Different reducing agents and ligand molecules can adjust the rate of redox reaction, while the alkali concentration and ligand molecules affect the rate of precipitation reaction (Figure 2b) [22-26]. Changing the reaction rate can reduce or increase the supersaturation of Cu_2O, thus controlling the crystallization process of Cu_2O. According to the chemical bonding theory of single crystal growth, the thermodynamic stable morphology of Cu_2O is octahedron [27,28]. The change of crystallization kinetics leads to the formation of kinetics-stable morphologies of cube and truncated octahedron (Figure 2b). In traditional materials synthesis, preferentially adsorbed molecular species were used to control exposed facets [29]. The use of chemical reaction to control the morphologies may be an easy nanofabrication route for fast screening of advanced electrode materials.

By adjusting the equilibrium between complexation, precipitation and redox reactions in liquid-phase crystallization, Cu_2O micro/nanocrystals with different morphologies were synthesized, i.e., hopper cube, cube, octahedron, rhombic dodecahedra, truncated octahedron, hollow octahedron etc., as shown in Figure 3a and b [30-34]. Based on hard and soft acid-base theory, a chemoaffinity-mediated crystallization strategy was presented to fabricate Cu_2O micro/nanocrystals by utilizing different Lewis base of OH^-, SO_4^{2-}, NO_3^-, Ac^- and Cl^- and Lewis acid of Cu^{2+}. The pH-controlled precursor formation–crystallization route has been designed to crystallize Cu_2O with systematic shape evolution from nanowire to cube and octahedron. These liquid-phase chemical reaction controlled synthesis method provided a novel synthesis route for the crystallization of metal and metal oxide materials with controllable morphologies.

Low temperature and in-situ electrochemical reaction routes have been designed for the synthesis of
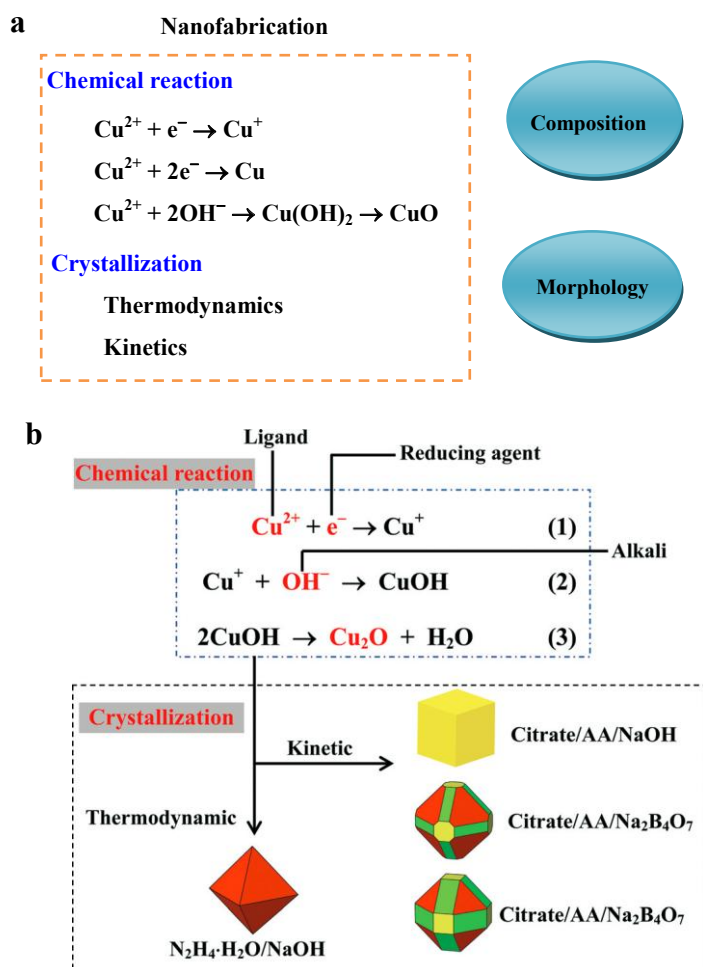
Figure 2 (a) Nanofabrication of Cu-based compounds with controllable compositions and morphologies by designing proper chemical reactions. (b) Chemical reaction and crystallization process to CuO nanocrystals. Reprinted with permission from Ref. [22].

high-performance Cu-based compounds. Various CuO morphologies i.e., nanoribbons, nanowires, nanosheets and nanoparticles aggregation have been crystallized by designing mechanochemical reactions route, room-temperature chemical transformation route and in-situ electrochemical reaction (Figure 3c-g) [35-37].

By controlling in-situ solid-phase chemical and electrochemical reactions, single-crystal CuO sheets were transformed into nanoparticles aggregation in CuO-Cu integrated anodes, leading to the production of many electroactive sites and the enhancement of electrochemical performance (Figure 3e and f) [35]. After 110 cycles, the discharge capacity of CuO-Cu integrated anode retains a large value of 706 mAh g^{-1}, which is beyond the theoretical capacity of CuO materials (674 mAh g^{-1}). The CuO-Cu integrated anode maintaining the high capacity and cycling stability owe to the following reasons: (1) the in-situ formed reactive nanoparticles under electrochemical reactions, (2) the active grains with size < 10 nm are interconnected and form a continuous network within CuO-Cu integrated anode, which provides a short pathway for local electron transport, (3) the abundant interface, formed between nanoparticles, provides a pathway for ionic transport and (4) the additional capacity of CuO anodes can be attributed to the release

of Cu from Cu current collector by in-situ electrochemical redox reaction.

Morphology-dependent electrochemical data of CuO electrode materials for Li-ion battery are shown in Table 1. CuO materials with different morphologies, sizes as well as synthesis methods can influence their electrochemical performances. Therefore, it is important to develop easy nanofabrication method to screen these electrode materials.

2.2 Mn-based electrode materials

MnO_2 material has attracted significant interests in electrochemical energy storage devices, such as Li-ion battery, Zn-Mn battery, supercapacitor, owing to its low cost, environmental compatibility and abundant polymorphism [48-50]. MnO_2 material possesses multiple tunnel and layered crystal structures, i.e., α, β, γ, δ-phases, etc. [51,52] b-MnO_2 possesses corner-sharing octahedral [MnO_6] units forming 1×1 tunnel structure with the tunnel size of 0.23 × 0.23 nm. a-MnO_2 includes 2×2 tunnel structure with the size of 0.46 × 0.46 nm, which can accommodate large-size ions, such as K$^+$ (0.133 nm) [53]. Nanostructured MnO_2 with various growth shapes such as wire-, plate-,
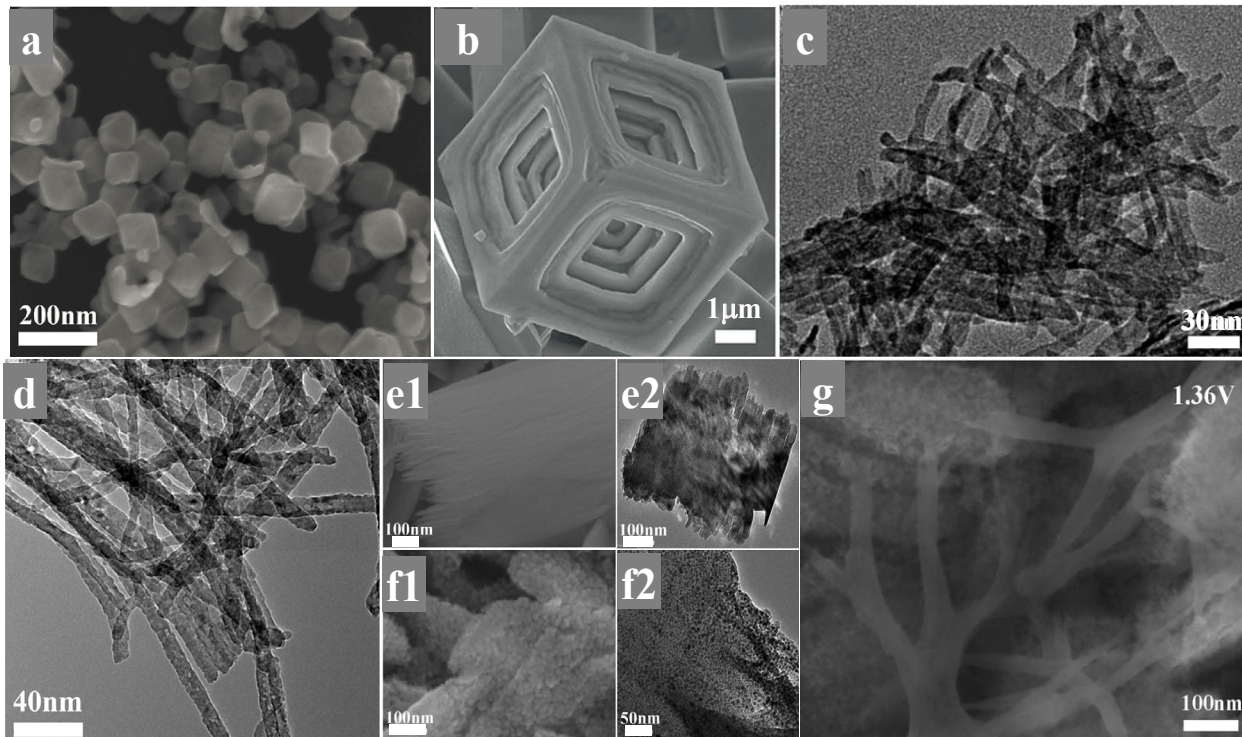
Figure 3 Various morphologies of Cu-based materials. (a) Cu_2O hollow octahedron, Reprinted with permission from Ref. [33]. (b) Cu_2O hopper cube, Reprinted with permission from Ref. [30]. (c) CuO nanoribbons, Reprinted with permission from Ref. [25]. (d) CuO nanowires, Reprinted with permission from Ref. [24]. (e, f) CuO nanosheets, Reprinted with permission from Ref. [35]. (g) nanowires in converted CuO nanosheets, Reprinted with permission from Ref. [36].

Table 1 Morphologies, sizes and electrochemical performances of CuO electrode materials for Li-ion battery. Reprinted with permission from Ref. [23].

Morphology	Particle size /nm	Method and reagent	Current rate/ mA g^{-1}	1st capacity / mAh g^{-1}	Capacity / mAh g^{-1} after n cycles
Urchin-like	153±13	Cu$_2$O oxidation, Cu$_2$O+ NH$_3$×H$_2$O	150	~800	560 (50)[38]
Nanoribbons arrays on copper sheet	1.2mm long	wet-chemical method, CuSO$_4$+NaOH	175	866	608 (275)[39]
CuO NWs*	7±3	Heating Cu(OH)$_2$ NWs	67	~1100	360.7 (50)[40]
Mesoporous CuO-CNTs* compositions	110 long, 34 short axis	60ºC heating Cu(NO$_3$)$_2$+ NH$_3$×H$_2$O+CNTs	0.1 C*	1160	650 (100)[41]
Dandelion-like	2-4 mm, 50nm	60ºC heating CuAc$_2$+ NH$_3$×H$_2$O	0.1 C	927	400 (50)[42]
Cog-shaped microparticles on Cu sheet	10nm nanowires	Cu oxidation, Cu+ (NH$_4$)$_2$S$_2$O$_8$ +NaOH+ NaAOT	0.05 C	1052	810 (10)[43]
Polycrystalline nanowires	20-40	wet-chemical method, CuSO$_4$+NaOH	0.05C	1040	650 (100)[44]
3D sponge-like CuO	~8	Cu NPs oxidation	0.1C	1200	~900 (50)[45]
1D pine-needle-like arrays on Cu sheet	270	Cu anodic oxidation and annealing	1C	~950	650 (100)[46]
Nanocrystalline-assembled Bundle-like	220	400ºC annealing Cu(OH)$_2$	0.3C	1179	666 (70)[47]

*NWs = nanowires; CNT = carbon nanotubes; 1C = 674 mA g^{-1}.
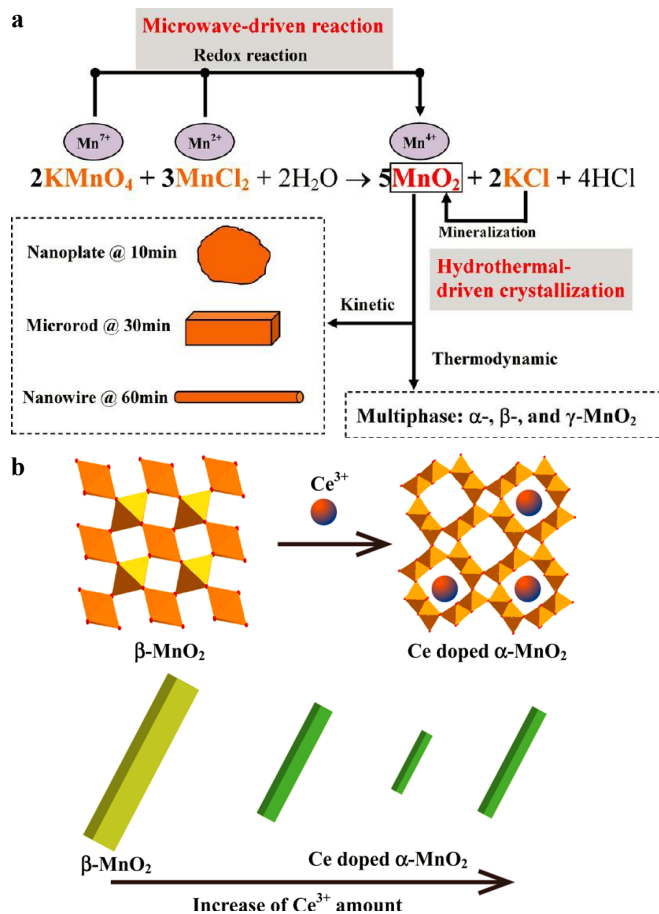
Figure 4 (a) Chemical reaction and crystallization design of MnO$_2$ materials. Reprinted with permission from Ref. [55]. (b) Schematic drawing of the phase transformation and size change of Ce-doped MnO$_2$ nanorods. Reprinted with permission from Ref. [58].

sphere-, rod-, and flower-like morphologies have been successfully fabricated by different synthesis methods [50]. They also display the morphology-dependent electrochemical performance. Therefore, finding fast synthesis method is also urgently needed to screen high-performance polymorphism.

Among various synthesis methods, microwave-hydrothermal technique is one kind of fast route, which can accelerate the finding rate of advanced electrode materials [54]. Microwave-hydrothermal method not only decreases the reaction time from several hours or even days down to 30 min, but also keeps the morphology controllability. For example, coupled with chemical reaction and crystallization design between $MnCl_2$ and $KMnO_4$, α-, β-, and γ- MnO_2 with the plate-, rod-, and wire-like shapes have been crystallized (Figure 4a), which show polymorphism-dependent electrochemical performance [55]. As shown in Table 2, the electrochemical results show that the Faradaic reactivity sequence is α- > γ- > β-MnO_2, the intercalation–deintercalation reactivity follows the order of γ- > α- > β-MnO_2, the conversion reactivity obeys the order of γ- > α- > β-phase. Microwave-hydrothermal method is shown as a facile and efficient way to synthesize MnO_2 materials and to fast screen their performances.

Doping is one of key methods to modify the physical and chemical properties of functional oxide materials [56,57]. It is reported that K^+ ions (0.133 nm) can stabilize MnO_2 with large tunnel or layer structures. Ce^{3+}/Ce^{4+} with ionic radius of about 0.1 nm can induce the formation of α-MnO_2 with 2×2 tunnel structure. Indeed, doping Ce^{3+} ions induces the phase transformation from β- to α-phase MnO_2 (Figure 4b) [58]. MnO_2 nanorods were first decreased to 10-20 nm in length, then increased to 70 nm with the increase of the added Ce^{3+} ions. The specific capacitance of β-MnO_2 electrode materials is only 13.1 F g^1, while all specific capacitances of Ce^{3+}-doped α-MnO_2 samples are larger than b-MnO_2. The smallest sized a-MnO_2 electrode materials show the highest value of 101.1 F g^1. Specific capacitance of Ce^{3+}-doped MnO_2 electrode materials increased 10-fold compared with undoped MnO_2, while the charge transfer resistance of Ce-doped MnO_2 also

decreased. With the only addition of rare earth ions, MnO_2 polymorph can be controlled, which also increase the screen rate of electrode materials.

3 Fast nanofabrication methods

3.1 Novel burning synthesis for binary and ternary nanomaterials

The controllable synthesis of nanomaterials with unique structure, size and composition often require more specialized synthesis approaches. Nowadays, energy-, envirmental- and time-cost are needed to consider during the choice of synthesis strategies. Hydrothermal, electrodeposition, microwave and sol-gel methods have been considered as greener and economic methods [59,60]. However, for the selecting fast nanofabrication method, combustion synthsis is the first choice, which also shows additional bonuses: (I) the combustion exothermic reaction provides the required reaction energy, once ignited without the need of external energy input, (II) the reaction time is short (usually seconds), (III) only needing simple equipment and environmentally friendly chemicals [61,62]. Compared with solid-phase combustion, the solution combustion synthesis can synthesize composite-controllable oxides, but it needs to select fuel molecules and often produce large volume changes during combustion (Figure 5a) [63]. A general and fast combustion method with using filter paper, methanol and metal nitrate as precursors was developed, which can synthesize metal, binary and ternary metal oxides (Figure 5b) [64].

In the filter paper burning process, the time spent from igniting to complete reaction is 12 s (Figure 6). Three different burning stages were found: burning of methanol, burning of filter paper, and burning without flame. The entire process of forming the oxide material involves the filter paper soaked with a methanol solution containing nitrate salt, and the combustion of the filter paper-nitrate salt. The filter paper acts as a constraint matrix to fix the metal ions and form nanoparticles with controllable size

Table 2. Synthetic conditions and discharge capacities of MnO_2 polymorphism for Li-ion batteries.

Reaction condition	Phase	Morphology	Anode 30th capacity (mAh/g)	Cathode 30th capacity (mAh/g)
MH at 160 ºC for 1h	β (dominant)	rod	150.2	26.4
MH at 160 ºC for 10 min	γ (dominant)	wire+plate	205.9	68.0
MH at 160 ºC for 20 min	β- (dominant)	rod+wire+plate	220.7	43.3
MH at 160 ºC for 1h (pH=2)	α	wire	116.9	33.8

a **Filter-paper combustion synthesis**

More fast reaction
Without additional treatment
Well-controlled particle size
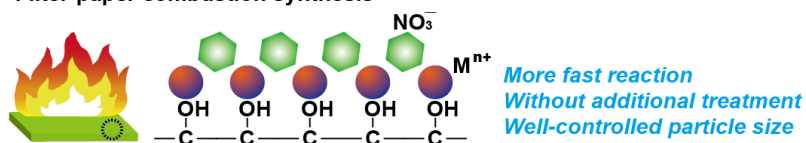
Time/energy efficiency
Well-developed porosity
From metal to ternary, quaternary oxides
Metastable materials
In-situ doping and functionality

Need high ignite temperature
Select specific fuel molecule
Large volume change during burn

Solution combustion synthesis

b

Filter paper

$M(NO_3)_x$ + Methanol

Methanol burning decomposition of $M(NO_3)_x$

Cellulose burning decomposition of $M(NO_3)_x$/filter paper

Glowing burning formation of final oxide

MO_x/M or MO_x
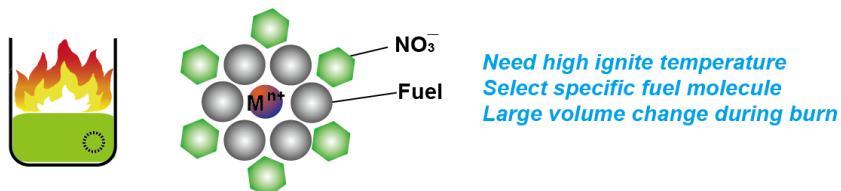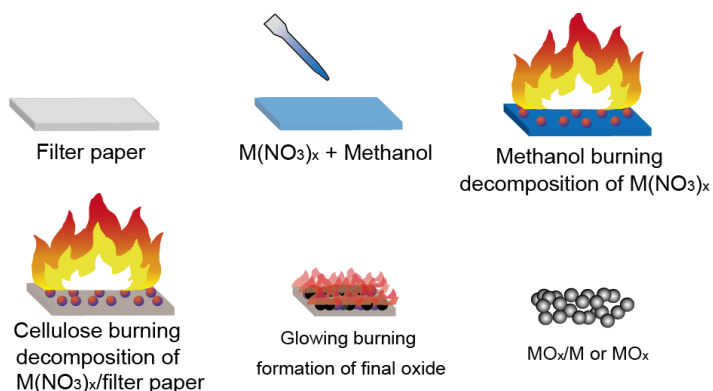
Figure 5 Schematic drawing of fast combustion process. (a) Advantages of filter-paper combustion synthesis compared with solution combustion. (b) Schematic illustration of 12 s combustion processes to synthesize metal oxides. Reprinted with permission from Ref. [64].

Burning of methanol

0 s 1 s 2 s

Burning of filter paper

3s 4 s 5s 6 s 7 s

Burning without flame

8 s 9 s 10 s 11 s 12 s

Figure 6 Digital photographs show the burning process with 0.1 M $Cu(NO_3)_2$ as copper salt. Reprinted with permission from Ref. [64].

of ~10-20 nm. The combustion method is general. A variety of metal, binary (MO_x) and ternary (ABO_3, A_2BO_4) oxides were synthesized with corresponding metal nitrates as precursor, $M(NO_3)_x$ (M= Fe^{3+}, Co^{2+}, Ni^{2+}, La^{3+}, Ce^{3+}, Pr^{3+}, Nd^{3+}, Er^{3+}, Tm^{3+}, Yb^{3+}, Lu^{3+}). The synthesized binary transition metal oxides and rare earth oxides included gamma-Fe_2O_3, CoO, NiO and Ln_2O_3 (Ln= La, Yb, Tm, Nd, Lu, Er), CeO_2, $PrO_{1.83}$. The thermodynamic reduction potential of the metal-nitrate-filter-paper burning system can be estimated in the range -0.26 and 1.72 V, which induce the occurrence of redox reactions of $Cu^{2+} \rightarrow Cu^+ \rightarrow Cu$, $Ni^{2+} \rightarrow$ Ni, $Co^{2+} \rightarrow Co^{3+}$, $Ce^{3+} \rightarrow Ce^{4+}$, $Pr^{3+} \rightarrow Pr^{4+}$. The filter-paper burning system can control the composite, oxidation state and size of final products in short 12 s.

Used as anode materials for Li-ion batteries, most as-burned metal oxides display high cycling stability (Figure 7a). The initial discharge capacity of CoO material is 949.3 mAh/g and the 50th capacity is 501.1 mAh/g, which can retain 71% reversible capacity (Figure 7b). The 60th reversible capacity for Cu_2O/CuO/Cu electrodes was 233 mAh/g, (Figure 7c and d), remaining 96 % of initial reversible capacity. Such a good electrochemical behavior

can be attributed to (1) tiny nanoparticles contributing to short electron/ion migration/diffusion length, (2) continuous conductive path providing fast electron transfer [64]. The burning route provides a fast screening method of advanced electrode materials.

3.2 Electrochemical exfoliation for 2D graphene

High conductive film electrodes can be applied for smart and flexible devices. Highly conductive inks are the best medium to fabricate highly conductive film by simple printing methods. Graphene ink is a promising candidate for the construction of high conductivity film owing to its 2D nature and unprecedented electrical conductivity [65-67]. The preparation route of graphene includes mechanical stripping method, epitaxial growth, chemical vapor deposition, Hummers method, solvent/surfactant assisted electrochemical exfoliation, etc. [68,69] However, these methods are difficult to synthesize graphene ink or need long synthesis cycle. The electrochemical exfoliation of graphite has received a great deal of attention due to
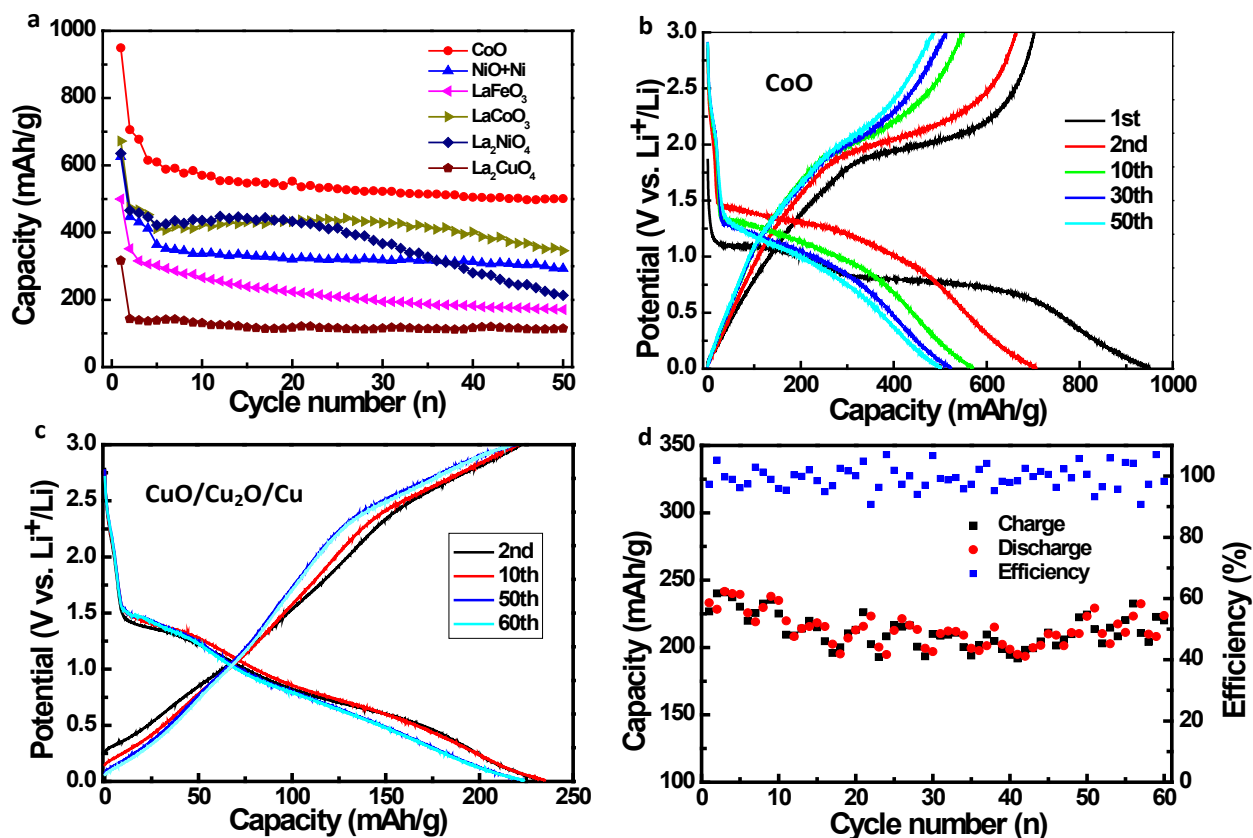
Figure 7 Li-ion battery anode performance of as-burned products. (a) Cycling performances at the current density of 100 mA/g. (b) Discharge-charge profiles of CoO anode at the current density of 100 mA/g. (c) Discharge-charge profiles and (d) cycling performance of the $CuO/Cu_2O/Cu$ anode at rate of 100 mA/g. Reprinted with permission from Ref. [64].

its ease of producing high quality graphene faster and greener [70,71]. We demonstrate that the electrochemical exfoliation of the pencil rod can form a well dispersed graphene ink in a fast route, which can be used to construct high conductivity film electrode [72].

The electrochemical exfoliation of the pencil core was carried out on a two-electrode system by using a pencil core and graphite sheet as anode and cathode (Figure 8). The electrolyte is 0.1 M $(NH_4)_2SO_4$ solution, which is greener than the previously used aqueous acids (such as sulfuric acid, phosphoric acid) and ionic liquids. Applied with 10 V bias, a large number of bubbles are formed at the electrode and pencil core begin to exfoliate. Interestingly, peeling products migrate to the top of the electrolyte, which is attributed to the effect of nanoclay in pencil rod. As shown in Figure 8e, the pencil core includes many thick graphite sheets. After exfoliation, fluffy wrinkled sheet aggregates were found, indicating the formation of graphene (Figure 8f). The current electrochemical oxidation process has several advantages, such as simplicity, high productivity, economical feasibility and short processing time (< 1 h).

The exfoliated graphene is well dispersed into ethanol solution to form graphene ink. Graphene ink can coat on Cu current collector or filter paper by printing (Figure 9a). The conductive graphene filter paper showed low resistance of 33 ohm/square, indicating it can serve as both current collector and electrode materials. The first discharge capacity was 586.4 mAh/g, and the 2nd charge and discharge capacities were 233.8 and 264.6 mAh/g, respectively, with coulombic efficiency of 88.4% (Figure 9b and 9c). From 3rd cycle, coulombic efficiencies are above 93%. The reversible capacity remains at 201.6 mAh/g and the coulombic efficiency is 98.5% after 50 cycles. Exfoliated graphene materials from 5B, 6B and 4B pencil rods show higher capacity than other electrodes (Figure 9d). The specific capacitance of 5B graphene supercapacitor was 21.4 F/g at the current density of 1 A/g (Figure 9e and 9f). The exfoliated graphene from pencil rod shows 3.5-fold increase in capacitance than that of pencil trace.

4 In-situ activation of colloidal electrode

The conventional design strategy for electrode materials mainly focused on the synthesis of amorphous or crystalline materials by controlling the synthesis methods (Figure 1c) [73-75]. Although these strategies can improve their electrochemical properties, the as-synthesized electrode materials cannot be fully utilized because of
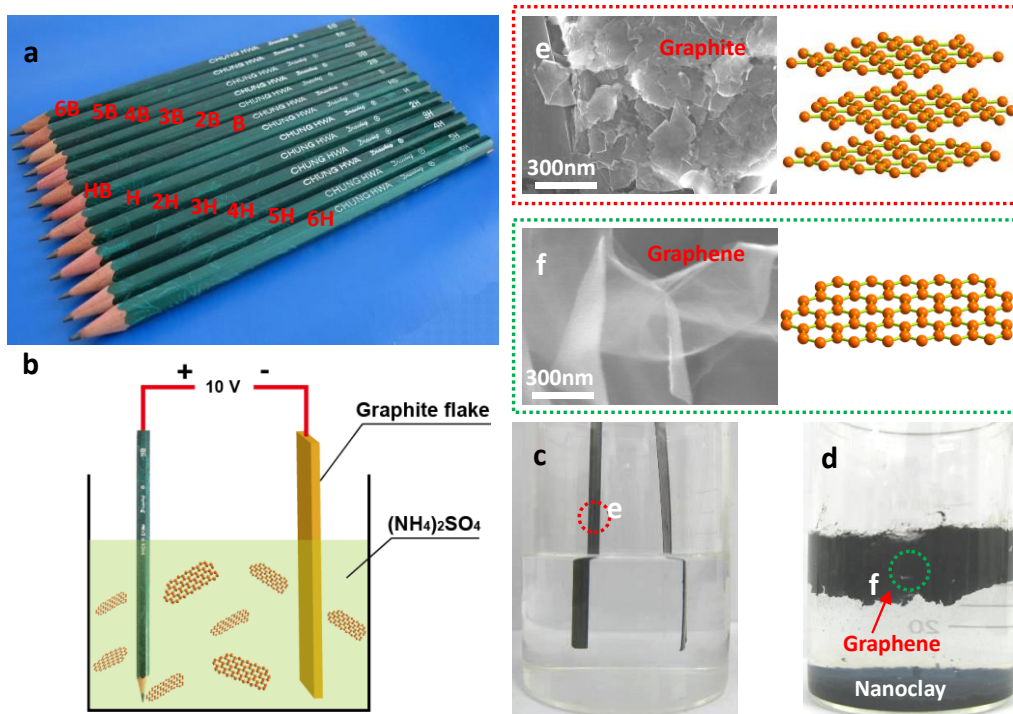
Figure 8 Electrochemical exfoliation of pencil leads to form graphene. (a) A set of pencils; (b and c) Electrochemical exfoliation experimental setup; (d) Photograph shows the condition after electrochemical exfoliation; SEM images of (e) pencil graphite and (f) exfoliated graphene
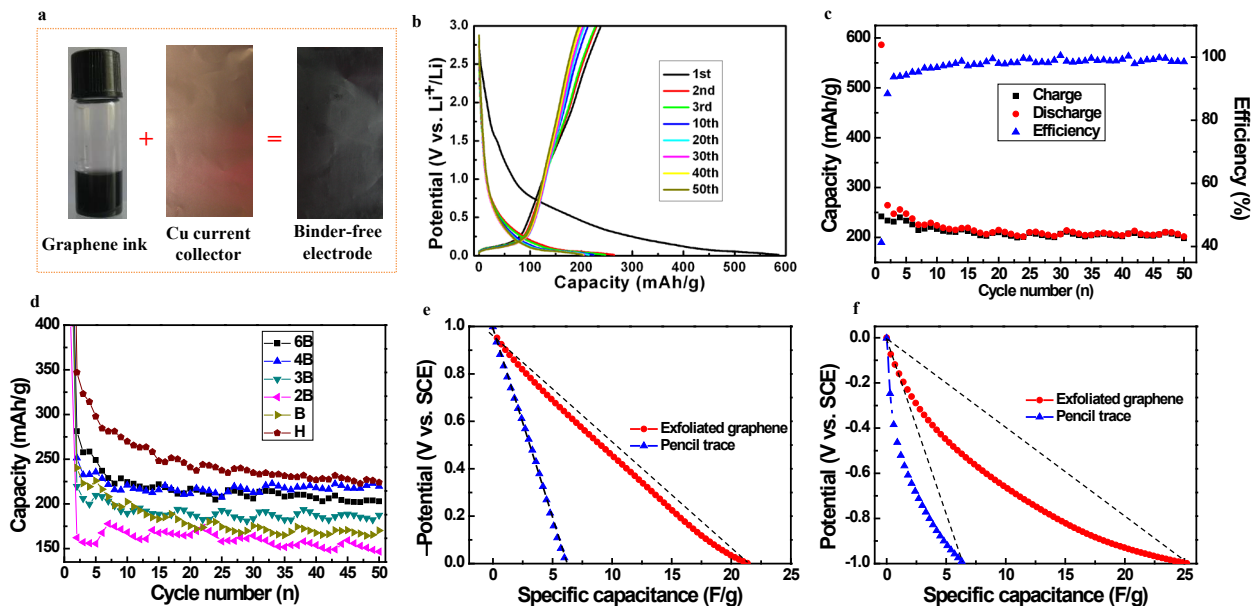
Figure 9 Electrochemical performances of the exfoliated graphene as Li-on batteries and supercapacitors. (a) Graphene ink and binder- and additive-free electrode coated on Cu foil. (b) Charge-discharge curves and (c and d) cycling performance of the exfoliated graphene from different pencil rods at current of 100 mA/g. (e) Discharge and (f) charge curves of the exfoliated graphene and pencil trace for supercapacitor. Reprinted with permission from Ref. [72].

the presence of electrochemical dead zone, leading to the capacitance lower than theoretical value [76]. To further improve their electrochemical performances, some electrode materials were in-situ grown on conductive substrates, i.e. carbon fiber, metal foam, which can shorten electron and ion transfer/diffusion length [77,78]. Instead, new attempts to increase the capacitance can be achieved by directly utilizing redoxable cations. How activate these cations is a challenge, which need innovative nanofabrication method [79]. Recently, in-situ formation of highly reactive colloids has been designed which can overcomes materials synthesis process (Figure 10a). The colloids in high reactive state can fully take advantage of the redox ability of cations, without the present of dead cations, leading to high specific capacitance. Compared with conventional electrode system (Figure 10b), colloid electrode system is high efficient for finding high-performance electrode.

Most as-obtained materials are applied in a variety of reactive and corrosive environments, and materials are likely to re-adjust their geometry and electronic structure to adapt the new environment [80]. For example, in Li-ion batteries, anode materials are transformed into polycrystalline structures after electrochemical cycling, which shows improved activity compared with original state [81]. However, conventional material synthesis and applications are generally separated in different environments, which often restrict their performance
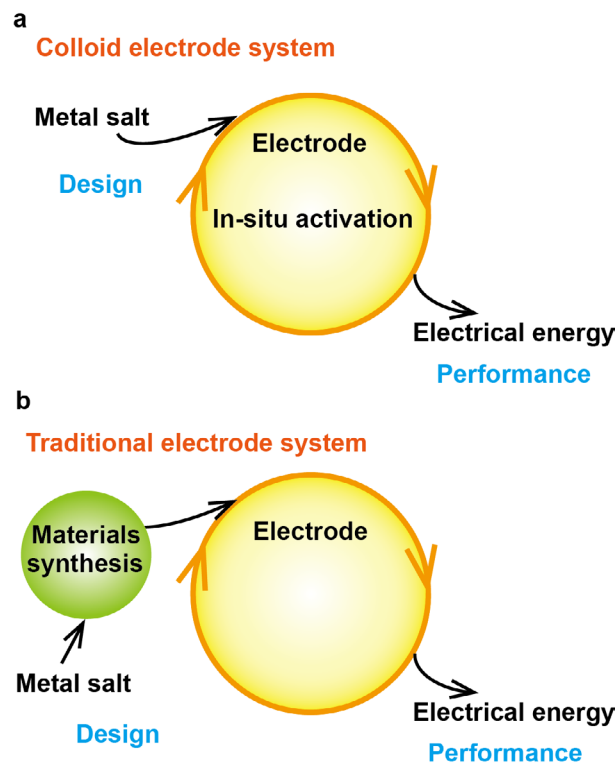
Figure 10 Comparison of colloidal electrode system and traditional electrode system. As one up-front design, colloid system can skip over the materials synthesis, accelerating screening rate of high-performance electrode.
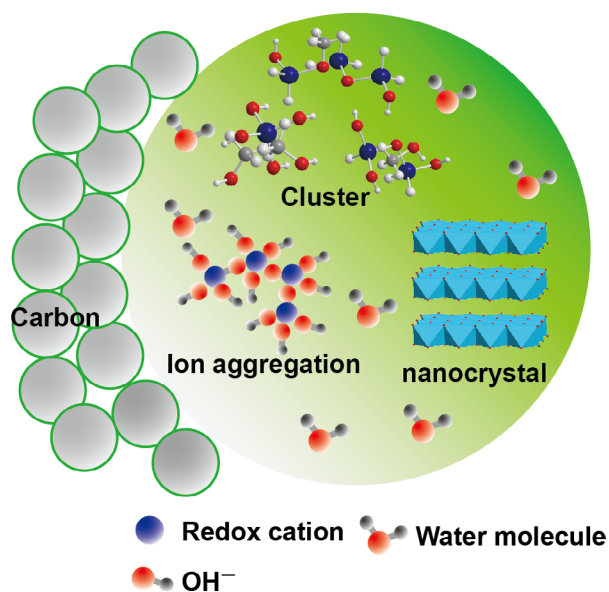
Figure 11 Schematic drawing of colloidal electrode system including multiple ions, clusters, aggregates, and multiple interactions, leading to abundant active centers for electrochemical redox reaction.

existing forms, i.e., colloidal clusters, ions, nanomaterials, and also includes a plurality of electrostatic interactions, van der Waals force and chemical bonding, which display the coincidence electrochemical behavior (Figure 11). The colloid system does not have a unique crystal structure, molecular configuration and clusters but with a specific reactivity structure relationship. Colloid system shows some unique characters: (1) large surface-to-volume ratio, (2) multiple varying forms of ions or cluster or aggregates, (3) complicated interaction coupled electrostatic, van der Waals and chemical bonding, (4) high chemical and electrochemical activity. Active colloidal electrode displays high capacitance. As shown in Table 1, the specific capacitance of the colloid electrode is higher than their theoretical one-electron value [85-93]. Because of the confined effect between colloids, carbon and binder, highly active redox cations and a large number of active centers formed in colloidal systems, thus leading to high capacitance. For detail discussion of colloid electrode, please read the references of [14, 83, 85].

Colloid electrodes also display promising potential for energy storage device application. Served as cathode of supercapattery device, V-based asymmetric device displays a high energy density of 50.4 Wh/kg at a power density of 250 W/kg (Figure 12a) [82]. The device still has

maximization. In-situ activation of electroactive colloid at the device scale can represent a new promising strategy to improve reactivity in same enviroment [82-84].

In redox ion level, colloidal system possesses multiple

Table 1 Theoretical and practical ionic capacitance of typical colloid systems, and their involved Faradaic reactions. Reprinted with permission from Ref. [18].

Active ion	Faradaic reaction	Theoretical ionic capacitance (F/g)	Practical ionic capacitance (F/g; initial salt)
V^{3+}	$V^{3+} \leftrightarrow V^{4+} + e^-$	3438 (0.55V, 1e)	4185 (VCl_3)
Mn^{2+}	$Mn^{3+} \leftrightarrow Mn^{4+} + e^-$	2192 (0.8V, 1e)	2518 ($MnCl_2$)
Fe^{3+}	$Fe^{2+} \leftrightarrow Fe^{3+} + e^-$	3833 (0.45V, 1e)	4729 ($FeCl_3$)
Co^{2+}	$Co^{2+} \leftrightarrow Co^{3+} + e^-$	3898 (0.42V, 1e)	1962 ($CoCl_2$)
Ni^{2+}	$Ni^{2+} \leftrightarrow Ni^{4+} + 2e^-$	7294 (0.45 V, 2e)	10286 ($NiCl_2$)
Cu^{2+}	$Cu^+ \leftrightarrow Cu^{2+} + e^-$	5061 (0.3V, 1e)	5442 ($CuCl_2$)
Sn^{4+}	$Sn^{4+} + 2e^- \leftrightarrow Sn^{2+}$	1803 (0.45V, e)	2241 ($SnCl_4$)
Ce^{3+}	$Ce^{3+} \leftrightarrow Ce^{4+} + e^-$	1719 (0.4V, 1e)	2060 ($Ce(NO_3)_3$)
Yb^{3+}	$Yb^{2+} \leftrightarrow Yb^{3+} + e^-$ $Yb \leftrightarrow Yb^{2+} + 2e^-$	1358 (0.41V, 1e) 2716 (0.41V, 2e)	2210 ($YbCl_3$)
Er^{3+}	$Er^{2+} \leftrightarrow Er^{3+} + e^-$ $Er^+ \leftrightarrow Er^{3+} + 2e^-$	1047 (0.55V, 1e) 2094 (0.55V, 2e)	1811 ($ErCl_3$)
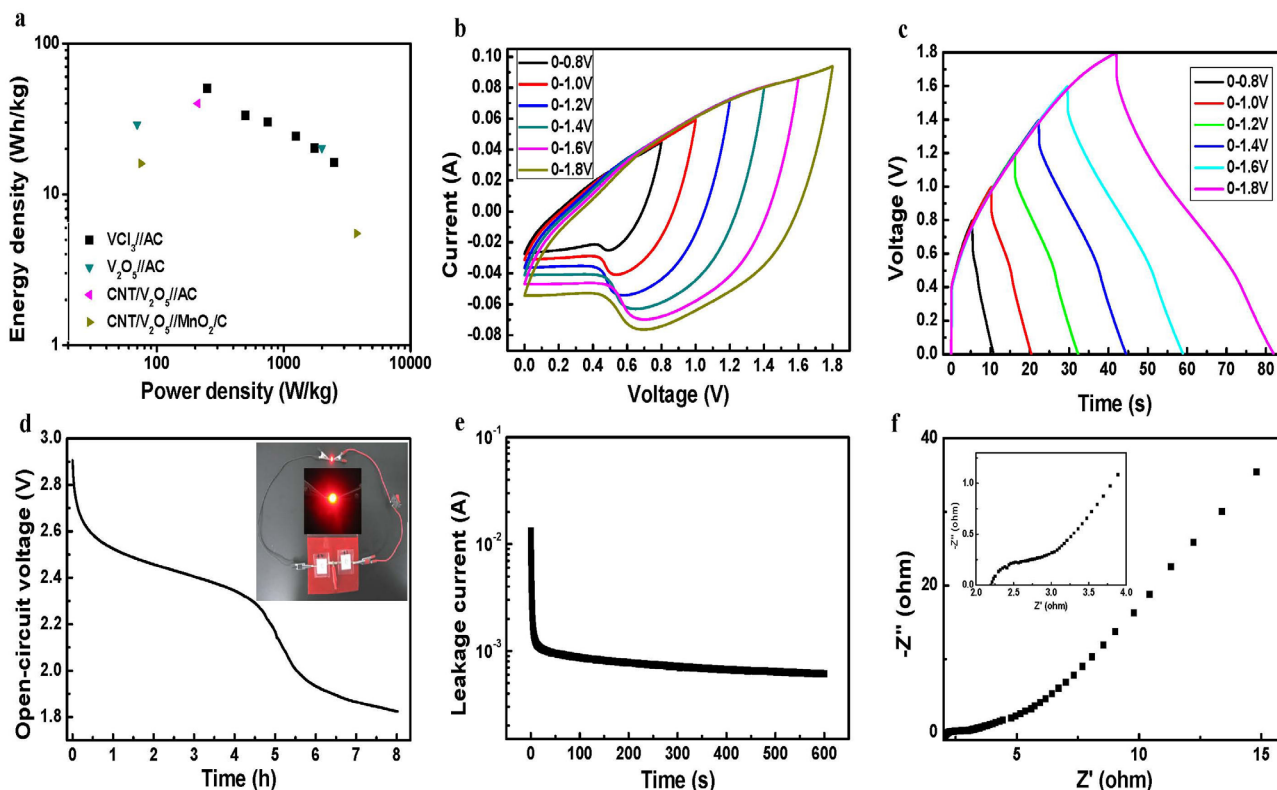
Figure 12 Electrochemical performances of V-colloid//AC asymmetric device. (a) Ragone plots, (b) CV curves at the sweep rate of 100 mV/s, (c) charge-discharge curves at the current density of 3 A/g. (d-f) Performance of two asymmetric devices connected in series, (d) self-discharge curves, (e) leakage current curve, (f) Nyquist plots. Inset of (d) is two asymmetric devices and LED indicator. Reprinted with permission from Ref. [82].

an energy density of 16.2 Wh/kg at the power density of 2500 W/kg. These values are comparable or higher than those of asymmetric V_2O_5//AC, CNT/V_2O_5 nanocomposite//AC, and CNT/V_2O_5 nanocomposite//MnO_2/C devices [82]. The voltage window can be extended to 1.8 V (Figure 12b and 12c). The two asymmetric devices are connected in series to drive the LED indicator (3 V). Self-discharge time from 3.6 to 1.8 V is 8h, approaching commercial value of supercapacitor. The leakage current of the asymmetrical devices was about 1 mA. A Low ESR value of 2.2 ohm allows rapid electron transport. Such excellent performance indicated that colloid supercapattery can show promising practical application value.

5 Summary and perspective

The rapidly developing energy society urgently needs the rapid screening of exceptional performance materials among lots of candidate electrode materials. The development of easy nanofabrication strategy for advanced electrode materials is one of promising solutions. This review outlined the advanced nanofabrication strategies for fast screening advanced electrode materials by optimizing control parameters. This contribution

encourages us to create innovative design ideas for rapid screening advanced electrode materials for energy storage devices. Despite much important progress, some important issues and challenges in future research need to be considered: function-directed precision design and synthesis of electrode materials, high throughput screening of high-performance electrode materials, atom- and ion-level nanofabrication, and smart nanofabrication for smart materials. The probable protocols to these challenges may include: as genetic engineering, we can design "gene coding", i.e. atom, ion, molecule to construct the electrode materials with specific active sites and atom arrangement; high throughput synthesis and characterization of electrode materials at one step is needed to satisfy the rapid screening of exceptional performance materials; the development of general and fast nanofabrication method is one direction; novel materials design idea is also needed. The up-front design, system integration design, and all-at-once design are good start, for example colloidal electrode system can skip over the material synthesis. With the progress of nanofabrication, function-oriented precision synthesis method based on atom- and ion-level for advanced energy storage materials will be springing up.

References

[1] Ghidiu M., Lukatskaya M. R., Zhao M. Q., Gogotsi Y., Barsoum M. W., Conductive two-dimensional titanium carbide 'clay' with high volumetric capacitance. Nature, 2014, 516, 78-81.

[2] Liu X., Huang J., Zhang Q., Mai L., Nanostructured metal oxides and sulfides for lithium−sulfur batteries. Adv. Mater., 2017, DOI: 10.1002/adma.201601759.

[3] Simon P., Gogotsi Y., Dunn B., Where do batteries end and supercapacitors begin.Science. 2014, 343, 1210-1211.

[4] Hercule K. M., Wei Q., Asare O. K., Qu L., Khan A. M., Yan M., Mai L., Interconnected nanorods−nanoflakes $Li_2Co_2(MoO_4)_3$ framework structure with enhanced electrochemical properties for supercapacitors. Adv. Energy Mater., 2015, 5, 1500060.

[5] Jia H., Lin J., Liu Y., Chen S., Cai Y., Lei J., Feng J., Fei W., Nanosized core−shell structured graphene−MnO_2 nanosheet arrays as stable electrodes for superior supercapacitors. J. Mater. Chem. A, 2017, DOI: 10.1039/C7TA02627g.

[6] Huang G. M., Zhao X. L., Li F., Zhang L. L., Zhang Y. X., Facile synthesis of ultrathin manganese dioxide nanosheets arrays on nickel foam as advanced binder-free supercapacitor electrodes. J. Power Sources, 2015, 277, 36−43.

[7] Sun H., Mei L., Liang J., Zhao Z., Lee C., Fei H., Ding M., Lau J., Li M., Wang C., Xu X., HSao G., Papandrea B., Shakir I., Dunn B., Huang Y., Duan X., Three-dimensional holey-graphene/niobia composite architectures for ultrahigh-rate energy storage. Science, 2017, 356, 599−604.

[8] Lu C., Wang D., Zhao J., Han S., Chen W., A continuous carbon nitride polyhedron assembly for high-performance flexible supercapacitors. Adv. Funct. Mater., 2017, 27, 1606219.

[9] Stauber T., Kohler H., Quasi-flat plasmonic bands in twisted bilayer graphene. Nano Lett., 2016, 16, 6844.

[10] Raji A., Salvatierra R., Kim N., Fan X., Li Y., Silva G., Sha J., Tour J., Lithium batteries with nearly maximum metal storage. ACS Nano, 2017, DOI: 10.1021/acsnano.7b02731.

[11] Liu Y, Wang Z., Zhong Y., Tade M., Zhou W., Shao Z., Molecular design of mesoporous $NiCo_2O_4$ and $NiCo_2S_4$ with sub-micrometer-polyhedron architectures for efficient pseudocapacitive energy storage. Adv. Funct. Mater., 2017, DOI: 10.1002/adfm.201701229.

[12] Durham J., Poyraz A., Takeuchi E., Marschilok A., Takeuchi K., Impact of multifunctional bimetallic materials on lithium battery electrochemistry. Acc. Chem. Res., 2016, 49, 1864−1872.

[13] Kundu D., Adams B., Duffort V., Vajargah S., Nazar L., A high-capacity and long-life aqueous rechargeable zinc battery using a metal oxide intercalation cathode. Nature Energy, 2016, 1, 16119.

[14] Chen K., Xue D., Materials chemistry toward electrochemical energy storage. J. Mater. Chem. A, 2016, 4, 7522−7537.

[15] Chen K., Song S., Xue D., Beyond graphene: materials chemistry toward high performance inorganic functional materials. J. Mater. Chem. A, 2015, 3, 2441−2453.

[16] Chen K., Li G., Xue D., Architecture engineering of supercapacitor electrode materials. Funct. Mater. Lett., 2016, 9, 1640001.

[17] Liu J., Xue D., Thermal oxidation strategy towards porous metal oxide hollow architectures. Adv. Mater., 2008, 20, 2622−2627.

[18] Chen K., Xue D., Rare earth and transitional metal colloidal supercapacitors. Sci. China Tech. Sci., 2015, 58, 1768−1778.

[19] Shang Y., Shao Y., Zhang D., et al., Recrystallization-induced self-assembly for the growth of Cu_2O superstructures. Angew. Chem. Int. Ed., 2014, 53, 11514−11518.

[20] Yao K. X., Yin X. M., Wang T. H., et al., Synthesis, self-assembly, disassembly, and reassembly of two types of Cu_2O nanocrystals unifaceted with {001} or {110} planes. J. Am. Chem. Soc., 2010, 132, 6131−6144.

[21] Xu J., Xue D., Five branching growth patterns in the cubic crystal system: A direct observation of cuprous oxide microcrystals. Acta Mater., 2007, 55, 2397-2406.

[22] Chen K., Song S., Xue D. Faceted Cu_2O structures with enhancing Li-ion battery anode performances. CrystEngComm, 2015, 17, 2110-2117.

[23] Chen K., Sun C., Xue D., Morphology engineering of high performance binary oxide electrodes. Phys. Chem. Chem. Phys., 2015, 17, 732-750.

[24] Chen K., Xue D., Room-temperature chemical transformation route to CuO nanowires toward high-performance electrode materials. J. Phys. Chem. C, 2013, 117, 22576-22583.

[25] Chen K., Xue D., A chemical reaction controlled mechano-chemical route to construction of CuO nanoribbons for high performance lithium-ion batteries. Phys. Chem. Chem. Phys., 2013, 15, 19708-19714.

[26] Chen K., Chemical reaction controlled synthesis of copper compounds and their materials performances, PhD thesis, Dalian University of Technology, Dalian, China, 2014.

[27] Zhao X., Bao Z., Sun C., Xue D., Polymorphology formation of Cu_2O: a microscopic understanding of single crystal growth from both thermodynamic and kinetic models. J. Cryst. Growth, 2009, 311, 711−715.

[28] Xue D., Li K., Liu J., Sun C., Chen K., Crystallization and functionality of inorganic materials. Mater. Res. Bull., 2012, 47, 2838−2842.

[29] Leng M., Liu M., Zhang Y., et al., Polyhedral 50-facet Cu_2O microc-rystals partially enclosed by {311} high-index planes: synthesis and enhanced catalytic CO oxidation activity. J. Am. Chem. Soc., 2010, 132, 17084−17087.

[30] Chen K., Song S., Xue D., Hopper-like framework growth evolution in a cubic system: a case study of Cu_2O. J. Appl. Crystallogr., 2013, 46, 1603-1609.

[31] Chen K., Xue D., pH-assisted crystallization of Cu_2O: chemical reactions control the evolution from nanowires to polyhedra. CrystEngComm, 2012, 14, 8068-8075.

[32] Chen K., Xue D., Chemoaffinity-mediated crystallization of Cu_2O: a reaction effect on crystal growth and anode property. CrystEngComm, 2013, 15, 1739-1746.

[33] Chen K., Song S., Xue D., Chemical reaction controlled synthesis of Cu_2O hollow octahedra and core-shell structures. CrystEngComm, 2013, 15, 10028-10033.

[34] Chen K., Sun C., Song S., et al. Polymorphic crystallization of Cu_2O compound. CrystEngComm, 2014, 16, 5257-5267.

[35] Chen K., Liu F., Xue D., et al. Beyond theoretical capacity in Cu-based integrated anode: insight into the structural evolution of CuO. J. Power Sources, 2015, 275, 136-143.

[36] Chen K., Xue D., Ex-situ identification of Cu$^+$ long-range diffusion path of Cu-based anode for lithium ion battery. Phys. Chem. Chem. Phys., 2014, 16, 11168-11172.

[37] Chen K., Song S., Xue D., Vapor-phase crystallization route to oxidized Cu foils in air as anode materials for lithium-ion batteries. CrystEngComm, 2013, 15, 144-151.

[38] Park J. C., Kim J., Kwon H., et al., Gram-scale synthesis of Cu$_2$O nanocubes and subsequent oxidation to CuO hollow nanostructures for lithium-ion battery anode materials. Adv. Mater., 2009, 21, 803-807.

[39] Ke F., Huang L., Wei G., et al., One-step fabrication of CuO nanoribbons array electrode and its excellent lithium storage performance. Electrochim. Acta, 2009, 54, 5825-5829.

[40] Huang H., Yu Q., Ye Y., et al., Thin copper oxide nanowires/ carbon nanotubes interpenetrating networks for lithium ion batteries. CrystEngComm, 2012, 14, 7294-7300.

[41] Ko S., Lee J., Yang H., et al., Mesoporous CuO particles threaded with CNTs for high-performance lithium-ion battery anodes. Adv. Mater., 2012, 24, 4451-4456.

[42] Xiang J. Y., Tu J. P., Zhang L., et al., Self-assembled synthesis of hierarchical nanostructured cuo with various morphologies and their application as anodes for lithium ion batteries. J. Power Sources, 2010, 19, 313-319.

[43] Zhang W., Li M., Wang Q., et al., Hierarchical self-assembly of microscale cog-like superstructures for enhanced performance in lithium-ion batteries. Adv. Funct. Mater., 2011, 21, 3516-3523.

[44] Chen L. B., Lu N., Xu C. M., et al., Electrochemical performance of polycrystalline CuO nanowires as anode material for Li ion batteries. Electrochim. Acta, 2009, 54, 4198-4201.

[45] Choi C. S., Park Y., Kim H., et al., Three-dimensional sponge-like architectured cupric oxides as high-power and long-life anode material for lithium rechargeable batteries. Electrochim. Acta, 2012, 70, 98-104.

[46] Chen X., Zhang N., Sun K., Facile fabrication of CuO 1D pine-needle-like arrays for super-rate lithium storage. J. Mater. Chem., 2012, 22, 15080-15084.

[47] Wang L., Cheng W., Gong H., et al., Facile synthesis of nanocrystalline-assembled bundle-like CuO nanostructure with high rate capacities and enhanced cycling stability as an anode material for lithium-ion batteries. J. Mater. Chem., 2012, 11297-11302.

[48] Kitchaev D. A., Dacek S. T., Sun W., Ceder G., Thermodynamics of phase selection in MnO$_2$ framework structures through alkali intercalation and hydration. J. Am. Chem. Soc. 2017, 139, 2672–2681.

[49] Yuan Y., Nie A., Odegard G. M., Xu R., Zhou D., Santhanagopalan S., He K., Asayesh-Ardakani H., Meng D. D., Klie R. F., Johnson C., Lu J., Shahbazian-Yassar R. Asynchronous crystal cell expansion during lithiation of K$^+$-stabilized α-MnO$_2$. Nano Lett., 2015, 15, 2998–3007.

[50] Wei W., Cui X., Chen W., Ivey D. G., Manganese oxide-based materials as electrochemical supercapacitor electrodes. Chem. Soc. Rev., 2011, 40, 1697–1721.

[51] Zhang Y., Sun C., Lu P., Li K., Song S. Xue D., Crystallization design of MnO$_2$ towards better supercapacitance. CrystEngComm, 2012, 14, 5892–5897.

[52] Zhang Y., Xue D., Mild synthesis route to nanostructured α-MnO$_2$ as electrode materials for electrochemical energy storage. Funct. Mater. Lett., 2012, 5, 1250030.

[53] Sun C., Zhang Y., Song S. Xue D., Tunnel-dependent supercapacitance of MnO$_2$: effects of crystal structure. J. Appl. Crystallogr., 2013, 46, 1128–1135.

[54] Li L., Guo Z., Du A., Liu H., Rapid microwave-assisted synthesis of Mn$_3$O$_4$–graphene nanocomposite and its lithium storage properties. J. Mater. Chem., 2012, 22, 3600–3605.

[55] Chen K., Noh Y., Li K., et al., Microwave-hydrothermal crystallization of polymorphic MnO$_2$ for electrochemical energy storage. J. Phys. Chem. C, 2013, 117, 10770-10779.

[56] Huang S., Wilson B. E., Wang B., Fang Y., Buffington K., Stein A., Truhlar D. G., Y-doped Li$_8$ZrO$_6$: A Li-ion battery cathode material with high capacity. J. Am. Chem. Soc., 2015, 137, 10992–11003.

[57] Zhu J., Liu G., Liu Z., Chu Z., Jin W., Xu N., Unprecedented perovskite oxyfluoride membranes with high-efficiency oxygen ion transport paths for low-temperature oxygen permeation. Adv. Mater., 2016, 28, 3511–3515.

[58] Chen K., Pan W., Xue D., Phase transformation of Ce^{3+}-doped MnO$_2$ for pseudocapacitive electrode materials. J. Phys. Chem. C, 2016, 120, 20077-20081.

[59] Wang H., Zhang J., Hang X., Zhang X., Xie J., Pan B., Xie Y., Half-metallicity in single-layered manganese dioxide nanosheets by defect engineering. Angew. Chem. Int. Ed., 2015, 54, 1195-1199.

[60] Zhang P., Yuan J., Fellinger T., Antonietti M., Li H., Wang Y., Improving hydrothermal carbonization by using poly(ionic liquid) s. Angew. Chem. Int. Ed., 2013, 52, 6028-6032.

[61] Li F., Ran J., Jaroniec M., Qiao S. Z., Solution combustion synthesis of metal oxide nanomaterials for energy storage and conversion. Nanoscale, 2015, 7, 17590–17610.

[62] Rajeshwar K., Tacconi N. R., Solution combustion synthesis of oxide semiconductors for solar energy conversion and environmental remediation. Chem. Soc. Rev., 2009, 38, 1984-1998.

[63] Koirala R., Pratsinis S. E., Baiker, A. synthesis of catalytic materials in flames: opportunities and challenges. Chem. Soc. Rev., 2016, 45, 3053-3068.

[64] Chen K., Xue D., Crystallization of transition metal oxides within 12 seconds. CrystEngComm, 2017, 19, 1230-1238.

[65] Liu F., Song S., Xue D., Zhang, H., Folded structured graphene paper for high performance electrode materials. Adv. Mater., 2012, 24, 1089-1094.

[66] Zhang Y., Chen P., Gao X., Wang B., Liu H., Wu H., Liu H., Dou S., Nitrogen-doped graphene ribbon assembled core−sheath MnO@graphene scrolls as hierarchically ordered 3d porous electrodes for fast and durable lithium storage. Adv. Funct. Mater., 2016, 26, 7754–7765.

[67] Chen K., Song S., Liu F., Xue D., Structural design of graphene for use in electrochemical energy storage devices. Chem. Soc. Rev. 2015, 44, 6230-6257.

[68] Shih C. J., Vijayaraghavan, A., Krishnan R., Sharma R., Han J. H., Ham M. H., Jin Z., Lin S. C., Paulus G. L. C., Reuel N. F., Wang Q. H., Blankschtein D., Strano M. S., Bi- and Trilayer Graphene Solutions. Nature Nanotechnol., 2011, 6, 439-445.

[69] Lee Y., Bae S., Jang H., Jang S., Zhu S. E., Sim S. H., Song Y. I., Hong B. H., Ahn J. H., Wafer-scale synthesis and transfer of graphene films. Nano Lett., 2010, 10, 490-493.

[70] Parvez K., Wu Z., Li R., Liu X., Graf, R., Feng, X., Müllen, K., Exfoliation of graphite into graphene in aqueous solutions of inorganic salts. J. Am. Chem. Soc., 2014, 136, 6083-6091.

[71] Chen K., Xue D. Preparation of colloidal graphene in quantity by electrochemical exfoliation. J. Colloid Interface Sci., 2014, 436, 41-46.

[72] Chen K., Xue D., Komarneni S., Nanoclay assisted electro-chemical exfoliation of pencil core to high conductive graphene thin-film electrode. J, Colloid Interface Sci., 2017, 487, 156-161.

[73] Wang H., Bai Y., Wu Q., Zhou W., Zhang H., Li J., Guo L., Rutile TiO_2 Nano-branched Arrays on FTO for Dye-sensitized Solar Cells, Phys. Chem. Chem. Phys., 2011, 13, 7008.

[74] Tu X., Luo S., Chen G., Li J., One-pot Synthesis, Characterization, and Enhanced Photocatalytic Activity of the BiOBr-Graphene Composites, Chem. Eur. J., 2012, 18, 14359-14366.

[75] Lu X. B., Zhou J., Zhao Y. H., Qiu Y., Li J., Room temperature ionic liquid based polystyrene nanofibers with superhydrophobility and conductivity produced by electrospinning, Chem. Mater., 2008, 20, 3420-3424.

[76] Long X., Wang Z., Xiao S., An Y., Yang S., Transition metal based layered double hydroxides tailored for energy conversion and storage. Mater. Today, 2016, 19, 213-226.

[77] Zhao J., Chen J., Xu S., Shao M., Yan D., Wei M., Evans D. G., Duan X., CoMn-layered double hydroxide nanowalls supported on carbon fibers for high-performance flexible energy storage devices. J. Mater. Chem. A, 2013, 1, 8836-8843.

[78] Li Y., Zhang L., Xiang X., Yan D., Li F., Engineering of ZnCo-layered double hydroxide nanowalls toward high-efficiency electro-chemical water oxidation. J. Mater. Chem. A, 2014, 2, 13250-13258.

[79] Huynh M., Shi C., Billinge S., Nocera D., Nature of activated manganese oxide for oxygen evolution. J. Am. Chem. Soc., 2015, 137, 14887–14904.

[80] Tao F., Dag S., Wang L., Liu Z., Butcher D. R., Bluhm H., Salmeron M., Somorjai G. A., Break-up of stepped platinum catalyst surfaces by high Co coverage. Science, 2010, 327, 850–863.

[81] Wang F., Robert R., Chernova N. A., Pereira N., Omenya F. , Badway F. , Hua X., Ruotolo M., Zhang R., Wu L., Volkov V., Su D., Key B., Whittingham M. S., Grey C. P., Amatucci G. G., Zhu Y., Graetz J., Conversion reaction mechanisms in lithium ion batteries: study of the binary metal fluoride electrodes. J. Am. Chem. Soc., 2011, 133, 18828–18836.

[82] Chen K., Xue D., High Energy Density Hybrid supercapacitor: in-situ functionalization of vanadium-based colloidal cathode. ACS Appl. Mater. Interfaces, 2016, 8, 29522-29528.

[83] Chen K., Xue D., Colloidal supercapacitor electrode materials. Mater. Res. Bull., 2016, 83, 201-206.

[84] Chen K., Xue D., In situ electrochemical activation of Ni-based colloids from an $NiCl_2$ electrode and their advanced energy storage performance. Nanoscale, 2016, 8, 17090–17095.

[85] Chen K., Xue D., Rare earth and transitional metal colloidal supercapacitors. Sci. China Technol. Sci., 2015, 58, 1768-1778.

[86] Chen X., Chen K., Wang H., Xue D., A colloidal pseudocapacitor: direct use of $Fe(NO_3)_3$ in electrode can lead to a high performance alkaline supercapacitor system. J. Colloid Interface Sci., 2015, 444, 49–57.

[87] Chen K., Xue D., Komarneni S., Colloidal pseudocapacitor: nanoscale aggregation of Mn colloids from $MnCl_2$ under alkaline condition. J. Power Sources, 2015, 279, 365-371.

[88] Chen K., Yin S., Xue D., Binary A_xB_{1-x} ionic alkaline pseudoca-pacitor system involving manganese, iron, cobalt, and nickel: formation of electroactive colloids via in-situ electric field assisted coprecipitation. Nanoscale, 2015, 7, 1161-1166.

[89] Chen K., Xue D., Ionic supercapacitor electrode materials: a system-level design of electrode and electrolyte for transforming ions into colloids. Colloids Interface Sci. Commun., 2014, 1, 39-42.

[90] Chen K., Song S., Xue D., An ionic aqueous pseudocapacitor system: electroactive ions in both salt-electrode and redox-electrolyte. RSC Adv., 2014, 4, 23338-23343.

[91] Chen K., Xue D., $YbCl_3$ electrode in alkaline aqueous electrolyte with high pseudocapacitance. J. Colloid Interface Sc., 2014, 424, 84-89.

[92] Chen K., Yang Y., Li K., Ma Z., Zhou Y., Xue D., $CoCl_2$ designed as excellent pseudocapacitor electrode materials. ACS Sustainable Chem. Eng., 2014, 2, 440−444.

[93] Chen K., Song S., Li K., Xue D., Water-soluble inorganic salts with ultrahigh specific capacitance: crystallization transformation investigation of $CuCl_2$ electrodes. CrystEngComm, 2013, 15, 10367-10373.

Authors' CV

Kunfeng Chen is a associate professor at Changchun Institute of Applied Chemistry, Chinese Academy of Sciences. He received his B. E. degree and Ph.D. in inorganic chemistry from Dalian University of Technology in 2009 and 2014. In 2015, he joined Changchun Institute of Applied Chemistry, Chinese Academy of Sciences as assistant professor. His research interests focus on electrochemical energy storage materials, and rare earth functional materials.

Dongfeng Xue is a full professor at Changchun Institute of Applied Chemistry, Chinese Academy of Sciences, where he received his Ph.D. (1998). In 2001, he was appointed as full professor in Dalian University of Technology. He has published over 430 papers in peer-reviewed journals (with h = 56), and more than 20 invited book chapters. He serves as the editorial membership of more than 20 international journals such as Materials Research Bulletin, Materials Research Innovations, Science of Advanced Materials, Journal of Porous Materials, Materials Focus, Energy and Environment Focus. His research interests include crystallography, crystallization, calculation and simulation of functional materials, chemical synthesis of condensed matters, and electrochemical energy storage.